Actuation Reading Insights
Estimating Shape and Forces in Tendon-Driven Slender Soft Robots

Feliu-Talegon, Daniel; Alkayas, Abdulaziz Y.; Adamu, Yusuf Abdullahi; Mathew, Anup Teejo; Renda, Federico

DOI
10.1109/TMECH.2025.3581774

Publication date
2025

Document Version
Final published version

Published in
IEEE/ASME Transactions on Mechatronics

Actuation Reading Insights: Estimating Shape and Forces in Tendon-Driven Slender Soft Robots

Daniel Feliu-Talegon, Abdulaziz Y. Alkayas, Yusuf Abdullahi Adamu, Anup Teejo Mathew, and Federico Renda

***Abstract*—Unlike traditional robots, soft robots can navigate narrow and complex environments while interacting safely and compliantly with their surroundings. The potential of these abilities motivates the development of algorithms that can accurately assess environmental interactions, making soft robots more autonomous. There is growing interest in estimating external loads in soft robots by matching precise shape data with mechanics models. This approach aims to enhance the robots' ability to adapt to unpredictable forces and environments, improving real-time decision-making and responses. In this article, we propose a novel approach for simultaneous shape and force estimation of tendon-driven slender soft robot-based solely on tendon displacements and tensions. Our approach introduces a kinetostatic model for slender soft robots based on the geometric variable-strain method, builds upon the Cosserat rod theory. The length of the threadlike actuators (tendons) is defined as a function of the deformation of the soft robot. By solving the inverse problem using this kinetostatic model and the length and tension of the tendons, we can estimate both the external force and the shape of the soft robot simultaneously. We validate our approach with an experimental prototype, achieving accurate force and shape estimation results. This method efficiently integrates actuation and sensing in a small and integrated form, which can be highly beneficial for applications requiring compact designs.**

***Index Terms*—Force estimation, geometric variable strain (GVS), kinetostatic model, shape estimation, soft robots.**

Received 11 February 2025; revised 11 May 2025; accepted 17 June 2025. Date of publication 14 July 2025; date of current version 30 December 2025. This work was supported in part by the US Office of Naval Research Global under Grant N62909- 21-1-2033 and in part by Khalifa University under Grant RIG-2023-048 and Grant RC1-2018-KUCARS. Recommended by Technical Editor A. K. Hoshiar and Senior Editor H. Wang. *(Corresponding author: Daniel Feliu-Talegon.)*

Daniel Feliu-Talegon is with the Mechanical and Nuclear Engineering Department, Khalifa University of Science and Technology, Abu Dhabi 127788, UAE, and also with the Cognitive Robotics Department, Delft University of Technology, 2600 GB Delft, The Netherlands (e-mail: daniel.talegon@ku.ac.ae).

Abdulaziz Y. Alkayas and Yusuf Abdullahi Adamu are with the Mechanical and Nuclear Engineering Department, Khalifa University of Science and Technology, Abu Dhabi 127788, UAE.

Anup Teejo Mathew and Federico Renda are with the Mechanical and Nuclear Engineering Department, Khalifa University of Science and Technology, Abu Dhabi 127788, UAE, and also with the Khalifa University Center for Autonomous Robotic Systems (KUCARS), Khalifa University, Abu Dhabi 127788, UAE.

Color versions of one or more figures in this article are available at https://doi.org/10.1109/TMECH.2025.3581774.

Digital Object Identifier 10.1109/TMECH.2025.3581774

I. Introduction

SOFT robots are increasingly becoming a crucial element in the design of robotic systems. Thanks to their compliant nature, soft robots complement their rigid counterparts by enabling safe interaction with humans and delicate environments, navigating through otherwise unreachable or confined spaces, and exhibiting greater resilience to external impacts. With advancements in materials, estimation algorithms, and control techniques, the capabilities of soft robots continue to expand, offering new possibilities for innovation in robotics [1]. Many works about soft robots have focused on developing models that describe the kinematics of these robots (i.e., robot's shape) given actuation inputs and external loads applied to the robot [2], [3]. It is well-known that external forces significantly influence the shape of these robots, making it essential to understand these forces to accurately predict the robot's shape. Consequently, force estimation becomes crucial for soft robots, enhancing safety, precision, and functionality in tasks, such as human–robot interaction, delicate handling, surgery, and tactile exploration. It supports advanced control, compliance regulation, and successful task execution by ensuring effective interaction and complementing shape sensing [4].

Typically, the robot's shape under various conditions is sensed using several distributed sensors integrated along its length [5], [6]. Different approaches for shape sensing estimation have been proposed. For instance, in [7] and [8], the pose (position and orientation) of certain markers is utilized for shape estimation, while in [9] optical fiber Bragg grating (FBG) sensors are employed.

In recent years, researchers have focused on estimating external forces applied to soft robots. Initially, the emphasis was on estimating the load under the assumption that the force is applied at the robot's tip. To address this, some studies have attached small load cell sensors at the tip of the robot [10], [11]. Other works propose to use six-axis load readings from a force sensor placed at the robot's base to estimate the force at the tip [12]. However, these approaches have the drawback of using bulky load cells, which are unsuitable for miniaturizing the size of the soft manipulators. Instead of sensing tip forces directly,

some research suggests investigating intrinsic tip force sensing for push–pull style continuum robots [13], [14]. These methods enable a significant reduction in the robot's size by using it as a multiaxis force sensor, which measures the reaction forces in the joints. In this context, Alkayas et al. [15] introduced an innovative technique for estimating the shape and tip forces of concentric tube robots by analyzing the displacements of the tubes and their reaction forces.

Other approaches utilize vision-based force estimation that first estimates the deformation of the continuum robot and then estimates the force using model-based methods [16] or 3-D curvature methods [17]. Although these approaches have proven to be efficient solutions for estimating tip forces, they require complementary vision systems, which increase the weight and complexity and are not suitable in scenarios with limited or cluttered visibility.

In addition, shape and tip force sensing has been extensively applied to catheter robots in minimally invasive surgery. For instance, Hasanzadeh and Janabi-Sharifi [18] proposed using a quasi-static model of a continuum robot to estimate the force at the tip based on the pose measurement of the catheter tip using an electromagnetic tracking system. Similarly, Khoshnam et al. [19] estimated the tip force by measuring the curvature of the flexible rod using a camera. To advance the development of small, flexible continuum robots for medical interventions [20], researchers have integrated FBG sensors for shape and force estimations, as demonstrated in [21] and [22].

Recent works have demonstrated that shape and force are coupled and should, therefore, be estimated simultaneously using statistically principled approaches. For instance, a probabilistic approach is explored to estimate tip force in [23]. To generalize these methods, researchers have moved beyond the tip force assumption to estimate multiple discrete loads along the continuum robot backbones [24], [25]. Moreover, simultaneous shape and distributed load estimation along a Cosserat rod were presented in [16] and later extended to tendon-driven continuum robots in [26]. In this direction, Ferguson et al. [27] proposed a method for simultaneous estimation of continuum robot shape and external loads using continuous batch estimation on a general robot model with actuation inputs. Although these methods have demonstrated excellent results in estimating distributed forces, they require expensive and bulky tracking devices with limited range and portability, and they suffer from occlusion problems. This motivates the exploration of different estimation methods using alternative sensing principles.

Significant progress has been made in cable-driven actuation for both actuation and shape estimation. Cable-driven actuation is one of the key mechanisms in soft and continuum robot [28], enabling compact and efficient actuation. Several studies have explored shape sensing based on tendon length, as demonstrated in [29] and [30]. By using multiple passive strings or tendons and measuring their lengths, these works estimate the shape of the continuum robot. Recent works [31], [32] proposed a dynamic model for cable-driven continuum robots, where the robot's morphology and driving state are determined solely using the cables measurements. Similarly, Wang et al. [33] collected multidimensional force/torque and cable tension data from the continuum robot. However, very few works have addressed the problem of estimating shape and forces simultaneously only using cable measurements, such as length and tension.

In learning-based approaches, Feng et al. [34] utilized cable tension and position as inputs to a neural network, proposing a method for estimating the tip contact force of continuum robots. While learning-based methods have shown promising results in various scenarios, they face challenges in generalizing to different conditions and fail when encountering new forces not considered during training. This limitation motivates the development of model-based methods for enhanced generalization capabilities.

In this context, to the best of the authors' knowledge, the only work to date that employs model-based approach and actuation readings for simultaneous shape and force estimation is presented in [35]. This work introduces an efficient method based on a precise model of a notched continuum surgical robot using the beam constraint model. The robot consists of multiple segments connected by compliant beams that bend only around a single axis perpendicular to the backbone, assuming no axial compression, elongation, or twisting deformation. While these assumptions may be reasonable for certain types of continuum robots, they become less applicable to slender, soft robots, which are the focus of our work. The main contributions of our work, compared with existing approaches in the literature, areas follows.

1) We propose a method for estimating shape and force-based solely on actuation readings, eliminating the need to integrate sensors into slender soft robots similar to [34] and [35]. Unlike [34], our approach generalizes to various force types and positions without requiring time-consuming training. In addition, it extends model-based methods, such as [35], to soft robots capable of bending, twisting, and elongating simultaneously. This is achieved using a kinetostatic model based on the geometric variable-strain (GVS) framework, accommodating multiple deformation modes within a unified approach. To the best of the authors' knowledge, this is the first model-based estimation method for slender soft robots relying solely on actuation readings.
2) We present a precise static modeling method for soft robots, capable of accurately predicting their 3-D morphology, including bending, torsion, and elongation/compression deformations—crucial for estimating external forces in 3-D space. Our approach also accounts for friction between tendons and guide holes, gravitational effects, and the influence of external loads.
3) We conduct sensitivity and resolution analyses of our approach with respect to sensing measurements and modeling errors to ensure its reliability in real-world applications.
4) We experimentally validate the accuracy of our model-based force-sensing method by applying 1-D and 3-D point forces at various locations in both planar and out-of-plane deformations, addressing the challenge of estimating forces tangential to the robot's backbone. Finally, we compare our results with simpler models, emphasizing

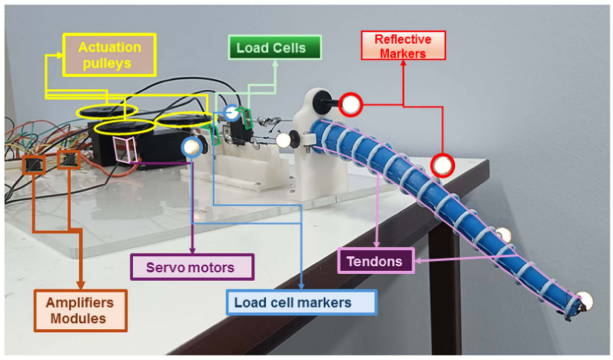

Fig. 1. Tendon-driven soft robot prototype.

the importance of incorporating bending, twisting, and elongation strains to enhance force estimation, particularly for out-of-plane deformations.

II. Design of a Soft Robot Utilizing Tendons for Integrated Sensing and Actuation

The proposed mechanism (see Fig. 1) features tendon-driven actuation, which effectively drives slender soft robots while also incorporating sensing capabilities for shape and force estimation. The system primarily consists of four components: a slender soft robot equipped with tendons, servo motors connected to pulleys to generate pulling movements for actuation, force sensors positioned between the motor systems and the tendons to measure their tensions, and the markers at the base of the tendons to measure the length of the tendons.

The slender soft robot comprises a 25 cm long conical manipulator with a circular cross-section fabricated with silicone (Smooth-On Mold Star 30 TM). In addition, several 3D-printed rigid rings are mounted along the soft manipulator to ensure the tendons are properly routed through them. This design choice helps to minimize friction between the tendons and the soft manipulator, enhancing the overall efficiency and performance of the system. The soft manipulator is equipped with three straight tendons that extend from the base to the tip of the soft manipulator. The tendons are phased 120° apart, enabling 3-D bending in all directions.

We use tendons made of Kevlar fiber, with a diameter of 0.5 mm, which exhibit negligible elongation within the operational range of our application. We tested them in the range of 0–15 N and observed no measurable elongation. This range is sufficient for our application; therefore, these tendons were selected for our experiments. It is crucial to note that, for our method, the tendons must not elongate to avoid influencing the friction direction and the measured length within the robot. The tendons are driven by servo motors (*Blue Bird BMS-A922+*) connected to pulleys, generating the pulling movements needed to actuate the system. Each tendon is attached to a commercial uniaxial force sensor (Micro S-type Load cell B313-20 N) that measures the tension forces in the tendons resulting from external loading. Each load cell is mounted on a 3D-printed part that allows it to slide with negligible friction through a linear rail.

TABLE I
Geometric and Technical Properties of the System Components

Soft Manipulator	
Radius at the base	12.5 mm
Radius at the tip	5 mm
Length of manipulator	250 mm
Material	Smooth-On Mold Star 3
Actuation	
Motors	Blue Bird BMS-A922+
Tendons routing	Linear
Number	3
Sensing	
Load cell	Micro S-type (B313-20N)
Number of cells	3
Tension routing	
Proximal radius, r_b	14 mm
Distal radius, r_t	6.5 mm
Range	$X \in [0, L]$
Tendon 1	$y = 0$ $z = r(X)$
Tendon 2	$y = -r(X)\cos(\pi/6)$; $z = -r(X)\sin(\pi/6)$
Tendon 3	$y = r(X)\cos(\pi/6)$; $z = -r(X)\sin(\pi/6)$

Actuator routing: $r(X) = r_b - (r_b - R_t)X/L$.

Every cell is connected to a HX711 amplifier module, which has been thoroughly calibrated to measure the tendon tension accurately. A highly precise camera system is used to monitor the various positions of the system through reflective markers. The camera system records the position of markers attached to the load cells to measure the variation in the length of the actuators. Although this measurement could be obtained from the servomotors, we opt for the tracking system due to its higher precision, with an accuracy of less than 0.1 mm. Furthermore, the positions of three markers located at the midpoint, three-quarters point, and the tip of the manipulator are recorded with the tracking system to verify the accuracy of our method in estimating the shape. The technical and geometric properties are provided in Table I.

III. Problem Formulation

In this section, we summarize the essential components of the GVS model used for simulating the dynamic response of a soft robot [36].

A. Kinematics of the Robot

A slender soft body can be modeled as a Cosserat rod, a continuous stack of rigid cross-sections parameterized by a curvilinear abscissa $X \in [0,\ L]$, where L is the length of the rod (see Fig. 2). The homogeneous transformation matrix corresponding to a coordinate frame attached to these cross-sections is defined as the directed spatial curve $\boldsymbol{g}(\bullet) : X \to \boldsymbol{g}(X) \in SE(3)$

$$\boldsymbol{g}(X) = \begin{bmatrix} \boldsymbol{R} & \boldsymbol{r} \\ \boldsymbol{0} & 1 \end{bmatrix} \tag{1}$$

where $\boldsymbol{r}(X) \in \mathbb{R}^3$ is the position of the local frame, while $\boldsymbol{R}(X) \in SO(3)$ provides the orientation of the local frame relative to the spatial frame. Strain $\boldsymbol{\xi}$ and velocity $\boldsymbol{\eta}$ twists of the body are defined by the partial derivative of (1) with respect

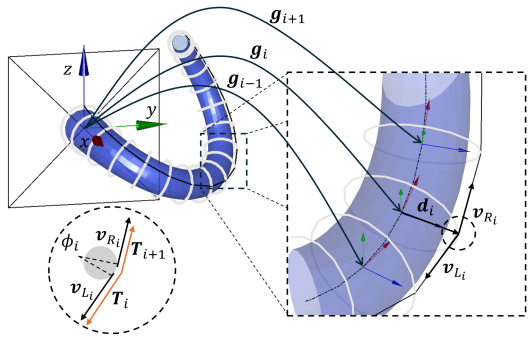

Fig. 2. Schematics of the manipulator with a single actuator.

to space $(\cdot)$ and time $\dot{(\cdot)}$

$$\boldsymbol{g}'(X) = \boldsymbol{g}\hat{\boldsymbol{\xi}}, \qquad \dot{\boldsymbol{g}}(X) = \boldsymbol{g}\hat{\boldsymbol{\eta}} \tag{2}$$

where $\hat{(\bullet)}$ indicates the isomorphism between $\mathbb{R}^6$ and $se(3)$. The relation between screw strain and velocity is established through the equality of the mixed partial derivatives in space and time

$$\boldsymbol{\eta}' = \dot{\boldsymbol{\xi}} - \mathrm{ad}_{\boldsymbol{\xi}}\boldsymbol{\eta} \tag{3}$$

where $\mathrm{ad}_{(\bullet)}$ is the adjoint operator of $se(3)$ (see the Appendix). Space integration of (2) (first part) and (3) provides

$$\boldsymbol{g}(X) = \exp\left(\widehat{\boldsymbol{\Omega}}(X)\right); \quad \boldsymbol{\eta}(X) = \mathrm{Ad}_{\boldsymbol{g}^{-1}} \int_0^X \mathrm{Ad}_{\boldsymbol{g}}\dot{\boldsymbol{\xi}} ds \tag{4}$$

where $\mathrm{Ad}_{\boldsymbol{g}}$ is the adjoint representation of $\boldsymbol{g}$ and $\boldsymbol{\Omega}(X)$ is the Magnus expansion of $\boldsymbol{\xi}(X)$. The GVS approach employs a finite set of strain bases to discretize the continuous strain field. The states of the system are introduced as generalized coordinates that span the strain bases

$$\boldsymbol{\xi}(X) = \boldsymbol{\Phi}_{\xi}(X)\boldsymbol{q} + \boldsymbol{\xi}^*(X) \tag{5}$$

where $\boldsymbol{\Phi}_{\xi}(X) \in \mathbb{R}^{6\times n_q}$ is the matrix function whose columns form the basis for the strain field and $\boldsymbol{q} \in \mathbb{R}^{n_q}$, where n_q being the DoFs, is the vector of generalized coordinates for the chosen basis function. Equation (5) can be substituted into (3), eventually leading to the definition of geometric Jacobian

$$\boldsymbol{\eta}(X) = \mathrm{Ad}^{-1}_{\boldsymbol{g}(X)} \int_0^X \mathrm{Ad}_{\boldsymbol{g}}\boldsymbol{\Phi}_{\xi} ds \dot{\boldsymbol{q}} = \boldsymbol{J}(\boldsymbol{q}, X)\dot{\boldsymbol{q}}. \tag{6}$$

Equations (4)–(6) are computed recursively by employing a quadrature approximation of the Magnus expansion $\boldsymbol{\Omega}$ (see the Appendix), as detailed in [37].

B. Statics and Actuation Model

Projecting the equilibrium equations of the Cosserat rod [38] using the geometric Jacobian through D'Alembert's principle leads to the standard equilibrium form

$$\boldsymbol{K}\boldsymbol{q} = \boldsymbol{B}(\boldsymbol{q})\boldsymbol{T} + \boldsymbol{F}(\boldsymbol{q}) \tag{7}$$

where $\boldsymbol{K}$ is the generalized stiffness matrix, $\boldsymbol{B}(\boldsymbol{q})$ is the generalized actuation basis, $\boldsymbol{T}$ is the vector of applied tendon tensions, and $\boldsymbol{F}(\boldsymbol{q})$ is the generalized external forces. We have

$$\boldsymbol{K} = \int_0^L \boldsymbol{\Phi}_{\xi}^T \boldsymbol{\Sigma} \boldsymbol{\Phi}_{\xi} dX \tag{8a}$$

$$\boldsymbol{F}(\boldsymbol{q}) = \int_0^L \boldsymbol{J}^T \overline{\boldsymbol{\mathcal{M}}} \mathrm{Ad}_{\boldsymbol{g}}^{-1} \boldsymbol{G} dX + \sum_{k=1}^{n_p} \boldsymbol{J}_k^T \mathrm{Ad}^*_{\boldsymbol{g}_{\theta}^{-1}} \boldsymbol{\mathcal{F}}_k \tag{8b}$$

where $\boldsymbol{\Sigma}$ is the screw elasticity matrix of a cross-section, n_p is the number of external point wrench, $\overline{\boldsymbol{\mathcal{M}}}\mathrm{Ad}_{\boldsymbol{g}}^{-1}\boldsymbol{G}$ is the distributed external force due to gravity, $\overline{\boldsymbol{\mathcal{M}}} = \rho\mathrm{diag}(J_x, J_y, J_z, A, A, A)$ is the screw inertia density matrix of the cross-section (ρ is the density, A is the cross-sectional area, and $J_{\bullet}$ is the second moment of area), $\boldsymbol{g}_{\theta}$ is the rotational component of $\boldsymbol{g}$, $\boldsymbol{G} = [\boldsymbol{0}^T \boldsymbol{a}_g^T]^T$, where $\boldsymbol{a}_g$ is the acceleration due to gravity in the global frame, and $\boldsymbol{\mathcal{F}}_k$ is the kth external point wrench, expressed in the global frame. For more comprehensive details about the implementation of the different components of (7), readers may refer to [39].

We now proceed to derive the generalized actuation basis and the formula for the length of the threadlike actuators. Consider the ith disk. The transformation matrix from the global frame to the frame at the rod's centerline corresponding to the disk is given by $\boldsymbol{g}_i$ (see Fig. 2). Hence, the position vector of the actuator at the disk location is given by $[\boldsymbol{r}_i^T, 1]^T = \boldsymbol{g}_i[\boldsymbol{d}_i^T, 1]^T$ being $\boldsymbol{d}_i = [0,\ y_i,\ z_i]^T$ is the local (cross-sectional) position of actuator. The kinematic equation relating the change in length of the actuator (y) with the state of the manipulator $\boldsymbol{q}$ is given by

$$y(\boldsymbol{q}) = \sum_{i=1}^{n_d-1} \|\boldsymbol{r}_{i+1} - \boldsymbol{r}_i\| - l^* \tag{9}$$

where n_d is the total number of disks and l^* is the reference length of the actuator (when $\boldsymbol{q} = 0$). The contact between the disks and the actuator involves friction, which can lead to tension loss. Hence, accurate modeling of tension loss at these contact points is crucial. To quantify this, we use the Capstan equation [40]

$$\frac{T_{i+1}}{T_i} = e^{-\mu\phi_i}; \qquad \phi_i = \cos^{-1}(-\boldsymbol{v}_{L_i}^T \boldsymbol{v}_{R_i}) \tag{10}$$

where μ is the coefficient of friction, i is the disk index, and $\boldsymbol{v}_L$ and $\boldsymbol{v}_R$ are unit vectors in the actuator directions on both sides of the guiding disk, expressed in the local frame (see Fig. 2)

$$\boldsymbol{v}_{L_i} = \boldsymbol{R}_i^T \frac{\boldsymbol{r}_{i-1} - \boldsymbol{r}_i}{\|\boldsymbol{r}_{i-1} - \boldsymbol{r}_i\|}; \quad \boldsymbol{v}_{R_i} = \boldsymbol{R}_i^T \frac{\boldsymbol{r}_{i+1} - \boldsymbol{r}_i}{\|\boldsymbol{r}_{i+1} - \boldsymbol{r}_i\|}. \tag{11}$$

Hence, the resultant actuation force at the location of the actuator on disk i is ($\boldsymbol{f}_i$) is given by

$$\boldsymbol{f}_i = \boldsymbol{v}_{L_i} T_i + \boldsymbol{v}_{R_i} T_{i+1} \tag{12}$$

where $\boldsymbol{f}_i$ can be considered a point force acting at the contact point. Notice that at the tip, $T_{i+1} = 0$. Using (10) and (12), we compute the point wrench on the manipulator's centerline at the

disk's location

$$\boldsymbol{\mathcal{F}}_i = \underbrace{\begin{pmatrix} \boldsymbol{d}_i \times \left(\boldsymbol{v}_{L_i} + \boldsymbol{v}_{R_i} e^{-\mu\phi_i}\right) \\ \boldsymbol{v}_{L_i} + \boldsymbol{v}_{R_i} e^{-\mu\phi_i} \end{pmatrix} e^{-\mu \sum_{j=1}^{i-1} \phi_j}}_{\boldsymbol{\Phi}_{a_i}} \cdot T. \tag{13}$$

Hence, the generalized actuation matrix is given by

$$\boldsymbol{B}(\boldsymbol{q}) = \sum_{i=1}^{n_d} \boldsymbol{J}_i^T \boldsymbol{\Phi}_{a_i}. \tag{14}$$

If there are n_a actuators, then $\boldsymbol{\Phi}_{a_i} = [\boldsymbol{\Phi}_{a_{i,1}}, \boldsymbol{\Phi}_{a_{i,2}}, \dots \boldsymbol{\Phi}_{a_{i,n_a}}]$, where $\boldsymbol{\Phi}_{a_{i,j}}$ corresponds to the actuation basis of jth actuator.

C. Forward Kinematics Problem

In this section, we present the problem formulation for determining the robot's shape in equilibrium, given specific actuator lengths and external forces applied to the robot. We use the soft robot model (7), which describes the statics of the system, along with the equation describing the length of the threadlike actuators $\boldsymbol{y}$. The proposed approach is able to compute the generalized coordinates $\boldsymbol{q}^{\epsilon}$ that define the manipulator's shape and tendon tensions $\boldsymbol{T}^{\epsilon}$ such that the actuator length $\boldsymbol{y}^{\epsilon}(\boldsymbol{q}^{\epsilon})$ match the measurements $\boldsymbol{y}$ and satisfy the static equilibrium model. Given the estimated generalized coordinates vector $\boldsymbol{q}^{\epsilon}$, we can define the error for the length measurement as

$$\boldsymbol{e}(\boldsymbol{q}^{\epsilon}) = \boldsymbol{y}^{\epsilon}(\boldsymbol{q}^{\epsilon}) - \boldsymbol{y}. \tag{15}$$

Then, we define the following minimization problem:

$$\begin{cases} \min_{\boldsymbol{q}^{\epsilon}, \boldsymbol{T}^{\epsilon}} & \|\boldsymbol{e}(\boldsymbol{q}^{\epsilon})\|_2^2 \\ \text{s.t.} & \boldsymbol{K}\boldsymbol{q}^{\epsilon} = \boldsymbol{B}(\boldsymbol{q}^{\epsilon})\boldsymbol{T}^{\epsilon} + \boldsymbol{F}(\boldsymbol{q}^{\epsilon}) \end{cases} \tag{16}$$

where the problem involves unknown variables $\boldsymbol{q}^{\epsilon}$ and $\boldsymbol{T}^{\epsilon}$.

D. Shape and Force Estimation Algorithm

We present the problem formulation to estimate the shape and external forces of slender soft robots using tendon displacement $\boldsymbol{y}$ and tension $\boldsymbol{T}$. Similarly to the forward kinematics problem, this approach estimates the generalized coordinates $\boldsymbol{q}^{\epsilon}$ and external forces $\boldsymbol{F}^{\epsilon}$ such that the actuator length $\boldsymbol{y}^{\epsilon}(\boldsymbol{q}^{\epsilon})$ matches the measurements $\boldsymbol{y}^{\boldsymbol{m}}$ and satisfies the static equilibrium model. We define the following minimization problem:

$$\begin{cases} \min_{\boldsymbol{q}^{\epsilon}, \boldsymbol{F}^{\epsilon}} & \|\boldsymbol{e}(\boldsymbol{q}^{\epsilon})\|_2^2 \\ \text{s.t.} & \boldsymbol{K}\boldsymbol{q}^{\epsilon} = \boldsymbol{B}(\boldsymbol{q}^{\epsilon})\boldsymbol{T} + \boldsymbol{F}^{\epsilon}(\boldsymbol{q}^{\epsilon}) \end{cases} \tag{17}$$

where the unknown variables of this minimization problem are the $\boldsymbol{q}^{\epsilon}$ and the magnitude of the forces $(n_q + n_p)$, and we have a system of equations of n_q plus n_a constraints, assuming that the external force's location is known. It is important to have enough actuators to estimate n_p forces, in principle $n_a \geq n_p$.

Remark 1: Notice from (8b) that by estimating $\boldsymbol{F}^{\epsilon}$ under the assumption that we know the force locations, we can compute $\boldsymbol{J}_k^T \mathrm{Ad}^*_{\boldsymbol{g}_\theta^{-1}}$ based on $\boldsymbol{q}^{\epsilon}$, and we only have to estimate $\boldsymbol{\mathcal{F}}_k$. This can be expressed as n_p forces of 1-D multiplied by a magnitude that we need to estimate. For example, a 3-D force can be decomposed into three 1-D forces for estimation.

IV. Simulation Results

In this section, we assess the estimation approach and its sensitivity to various measurements and parameters using a series of numerical simulations. In those simulations, a 0.25 m-long soft conical manipulator featuring a Young's modulus of 0.66 MPa, a density of 1121 kg/m^3, a Poisson ratio of 0.5, and a static friction of the tendons coefficient of 0.3 is considered. The circular cross section of the manipulator and the routing of the tendons were selected to match the experimental prototype (see Table I). The bases of our system are a constant Legendre polynomial basis for twisting, fourth-order Legendre polynomial basis for the two bending directions (y and z) and third-order Legendre polynomial basis for the elongation, resulting in a total of 15 DOFs.

We apply forces to the tip of the soft manipulator for different tendon lengths (forward kinematics problem) and compare the results with the estimation problem solution. In addition, we examine the sensitivity of our estimation algorithm to various factors to ensure its reliability in real-world applications. These factors include 1) inaccuracies in length measurement, 2) inaccuracies in tension measurement, and 3) inaccuracies in modeling friction in the tendons where we modify the friction coefficient μ. In the first analysis, we employ a single tendon (Tendon 1 of Table I) under a vertically downward force (negative global z direction). Then, we are using one tendon to estimate one unknown in a planar deformation. The objective is to estimate simultaneously the shape and the magnitude u_{p_1} of the force, assuming that $\boldsymbol{\mathcal{F}}_1 = [0, 0, 0, 0, 0, 1]^T u_{p_1}$ of (8b). To assess its sensibility, we introduce an error of ± 1 mm, ± 2.5 %, and ± 15 % for the length measurements, tension measurements, and the friction coefficient, respectively. Fig. 3(a) shows the estimation and the range of sensitivity for different forces -25, -75, and -125 gF for a range of increment of actuator length $\in [-0.02,\ 0]$ m. It can be noted that friction uncertainty impacts estimation performance similarly to tension uncertainty. This is because friction uncertainty can be effectively viewed as a loss of tension, as previously mentioned. The trend differs for the length case because an uncertainty of ± 1 mm has a greater impact compared to $y = -0.02$ m. The results show an average error of 12%, with a maximum error of 17% compared to the real force value in the case where there are inaccuracies in length measurement. In addition, the results indicate an average error of 8% with a maximum error of 10% in the case where there are inaccuracies in tension measurement and friction modeling.

In the second analysis, we employ a three-tendon manipulator (tendons routing of Table I) under a 3-D tip force. In this case, with measurements from three tendons, we can estimate all three components of the force. The objective is to estimate simultaneously the shape and the force magnitudes $\boldsymbol{u_p} = [u_{p_1}, u_{p_2}, u_{p_3}]$, assuming that $\boldsymbol{\mathcal{F}}_1 = [0, 0, 0, 1, 0, 0]^T u_{p_1}$, $\boldsymbol{\mathcal{F}}_2 = [0, 0, 0, 0, 1, 0]^T u_{p_2}$, and $\boldsymbol{\mathcal{F}}_3 = [0, 0, 0, 0, 0, 1]^T u_{p_3}$. In this case, we divide the amounts of uncertainties over the number of tendons and create all positive and negative combinations for each of the three tendons, resulting in 27 cases. Fig. 3(b) shows the estimation uncertainty ellipsoids for each applied force created from the 27 uncertainty combinations mentioned earlier. The colors represent the average estimation errors across

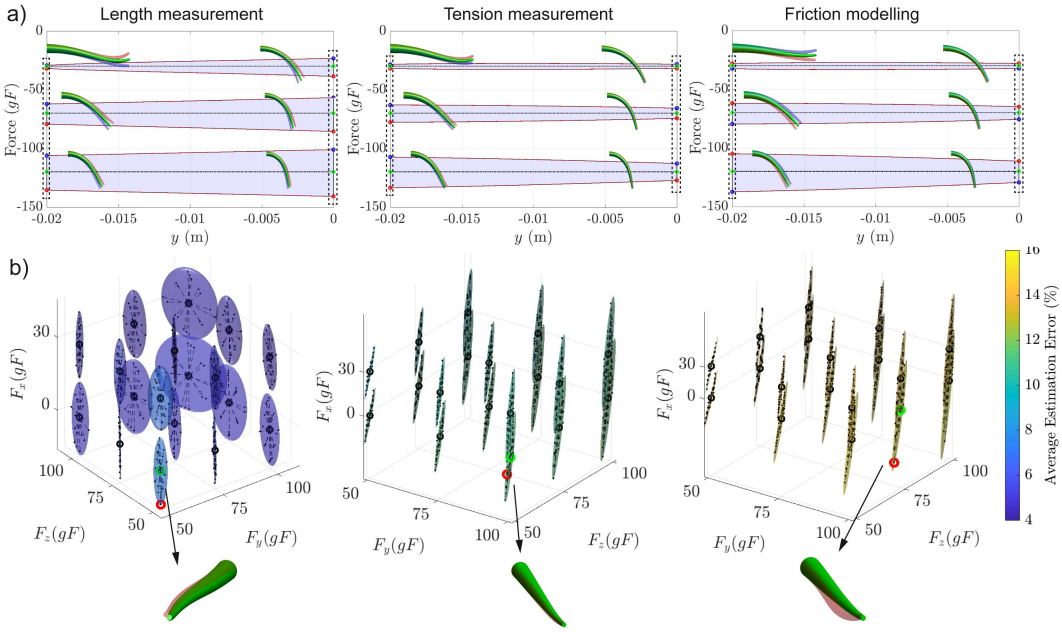

Fig. 3. Force estimation sensitivity analysis. (a) Estimation performance for single-tendon manipulator subjected to a vertical force (global frame). As inset, the configuration of the robots is shown at each extreme of $\boldsymbol{y}$, and each color is the configuration of the corresponding colored-circle estimated force value. (b) Estimation performance for a three-tendon manipulator under 3-D forces (global frame F_x, F_y, and F_z). The ellipsoids represent regions of estimation uncertainty. We also illustrate an example of the real shape (in green) and the estimated shape (in red) to demonstrate the sensitivity of the shape estimation. Black circles indicate the real force used in the forward kinematics problem, while the black dots are the estimated forces.

the 27 uncertainty combinations. It can be seen that, as concluded in the single-tendon case, uncertainties in tension and friction have almost the same effect on the estimation performance. This means that variations in the tension and friction coefficients significantly affect the value of F_x, making its estimation a more challenging task. We observe that average errors from inaccuracies in length measurements range from 4-8%, while errors due to inaccuracies in actuator tension measurement and friction modeling range from 12% to 16%.

We also performed a resolution analysis of our estimation method along each of the three external force directions. We have assumed that the tension sensor has a resolution of $\pm \frac{2.5}{3}\%$ of the tension measurement, and we examined how this sensor resolution affects the estimation of the different components of the 3-D force. Specifically, we identified the minimum increment in every force component that produces a detectable change in at least one of the tension components considering the mentioned resolution of the sensor. We have done this analysis through the whole range of forces used in this section. We found that the average resolution for each component across the full range is as follows: $[\Delta_x, \Delta_y, \Delta_z] = [3.72 \pm 3.6,\ 0.36 \pm 0.16,\ 0.46 \pm 0.2]$ g. We can see that the standard deviations are quite high compared to the average values, indicating that the resolution strongly depends on the robot's configuration. Moreover, these results indicate that the resolution of the F_x component is worse than that of the other components, as only average changes around 4 g can be detected, whereas in the other directions, changes as small as 0.5 g are detectable. This highlights the challenge of achieving accurate force estimation in soft robots, particularly along the robot's backbone. Although the forces are expressed in the global frame, the base frame orientation of the system causes the F_x component to project significantly along the backbone. As a result, accurately estimating F_x becomes more difficult. Note that the resolution in different directions depends on the base frame orientation, as it is influenced by both the robot's backbone orientation and the direction of gravity. However, these effects can still be analyzed using the same formulation by choosing a different base frame orientation.

These results validate the proposed approach, which allows for the estimation of 1-D and 3-D forces, along with their shapes, using one tendon and three tendons, respectively. Hence, as highlighted in Section III-D, to estimate n_p forces components, a sufficient number of tendons n_a is required, such that $n_a \geq n_p$. For instance, for the estimation of a 2-D force in the planar case, at least two tendons are needed to estimate the force components along each direction. Finally, the results show that introducing inaccuracies in the friction coefficient and measurements still enables precise force estimation, yielding an error of around 10% for the single-tendon (1-D) case and up to 15% for the three-tendon (3-D) case.

V. Experimental Results

In this section, the proposed estimation method is tested on the soft robot manipulator described in Section II. We tested the estimation method across various scenarios, conducting multiple trials where a single point 1-D/3-D force was applied at different locations, assuming the force's position was known. For each experiment, we calculate the root-mean-square error (RMSE) for the three markers positioned in different

points along the manipulator to quantify the error in shape estimation.

A. Static Model Identification

The accuracy of the force estimation produced by our method is highly dependent on the manipulator properties, such as Young's modulus, density, and tendon friction. Therefore, it is essential to accurately identify these values. To achieve this, we divided the process into two steps. First, the properties of the link (equivalent density and Young Modulus) are estimated by placing various weights at the tip without actuating the system. We then seek optimal parameters to minimize the difference between the real measured marker positions and those obtained using our kinetostatic model. Once these properties are determined, the tendon friction is calibrated by applying different tensions to the tendons and minimizing again the real measured marker positions and that obtained using our kinetostatic model. We validate the proposed model using the same basis utilized in the simulations, specifically the Legendre polynomial basis, with a total of 15 DOFs. The proposed identification method is based on the measurement of the three markers located at the midpoint, three-quarters point, and the tip of the manipulator in N sets of different experiments. A similar approach was presented in [41] to identify the parameters of the model. We define the error for the measurement in the mth marker and the snapshot kth as

$$\boldsymbol{e}_m^k(\boldsymbol{q}^{k,\mathfrak{e}}) = \boldsymbol{p}_m^k(\boldsymbol{q}^{k,\mathfrak{e}}) - \boldsymbol{p}_{\mathfrak{e},m}^k \tag{18}$$

where $\boldsymbol{p}_m^k$ and $\boldsymbol{p}_{\mathfrak{e},m}^k$ represent the marker positions measured and those estimated by the static model, respectively. Consequently, we define the following minimization problem:

$$\begin{cases} \min_{\boldsymbol{q}^{k,\mathfrak{e}},\boldsymbol{\Theta}} & \displaystyle\sum_{k=1}^{N} \|\boldsymbol{e}^k(\boldsymbol{q}^{k,\mathfrak{e}})\|_2^2 \\ \text{s.t.} & \boldsymbol{K}\boldsymbol{q}^{1,\mathfrak{e}} - \boldsymbol{B}(\boldsymbol{q}^{1,\mathfrak{e}})\boldsymbol{T}^1 - \boldsymbol{F}(\boldsymbol{q}^{1,\mathfrak{e}}) = \boldsymbol{0} \\ & \vdots \\ & \boldsymbol{K}\boldsymbol{q}^{N,\mathfrak{e}} - \boldsymbol{B}(\boldsymbol{q}^{N,\mathfrak{e}})\boldsymbol{T}^N - \boldsymbol{F}(\boldsymbol{q}^{N,\mathfrak{e}}) = \boldsymbol{0} \end{cases} \tag{19}$$

where $\boldsymbol{e} = [\boldsymbol{e}_1^T, \boldsymbol{e}_2^T, \ldots, \boldsymbol{e}_{n_m}^T]^T$, n_m is the number of markers, and $\boldsymbol{\Theta}$ represents the parameters to be identified. In our case, these parameters are the equivalent density and Young's modulus of the manipulator, as well as the static friction in the tendons. Then, material properties for the prototype were identified, yielding a Young's modulus of 1 MPa, a density of 1340 kg/m^3, and a friction coefficient of the actuators 0.4. The proposed model, using the obtained parameters, results in an average rms error of 5 mm, which is approximately 2% of the total length of the manipulator. These parameters and the proposed basis will then be used for the estimation approach in the experiments.

B. Shape and Force Sensing Method

To test our proposed shape and force sensing method, we conducted a series of experiments, which include: 1) using a single tendon to estimate the magnitude of the force in the direction of gravity for both planar and 3-D deformations, 2) using three tendons in 3-D deformation to estimate the 3-D force applied at the tip, and 3) estimating a distributed force along the robot.

1) Estimation 1-D External Point Forces: We now consider planar deformation using a single tendon (Tendon 1 of Table I) to estimate the magnitude of the force in the direction of gravity. In this case, the gravity force is known, and we estimate the magnitude of the applied force, assuming that the force location is known. During the experiments, we use different calibrated weights, which are attached to one of the rigid rings. For forces applied at the tip position, we use weights of 13, 18, 23, 28, and 33 g. For forces applied at intermediate points, we use weights of 65 and 120 g. We carried out several experiments where forces are applied at three points along the manipulator, X_f: the midpoint of the manipulator, three-quarters along its length, and the tip. Notice that the location of the force affects in (8b) the computation of $\boldsymbol{J}_k^T \mathrm{Ad}_{\boldsymbol{g}_\theta}^{-1}$. However, the problem inversion remains similar regardless of the location of the force, assuming that we know the location.

Moreover, we also use a single tendon not in the same plane as the force to create out-of-plane deformation (Tension 3 of Table I) to estimate the magnitude of an external point force in the direction of gravity while producing 3-D deformations. Table II presents the results for various point forces with different magnitudes and locations where the applied forces u_p^*, the estimated forces u_p, the error in the force estimation e_{u_p}, and the RMSE error in shape estimation are represented. Fig. 4 illustrates the deformation of the manipulator and the reconstructed shape achieved through our estimation method for different cases. The results show for the case of planar deformation, the average accuracy in force estimation is around 10%, and the average RMSE is approximately 12 mm. In the case of 3-D deformations, the average accuracy in force estimation is around 8%, and the average RMSE is about 10 mm, similar to the 2-D case.

2) Estimation 3-D External Point Forces: We also validate our approach with a more intricate scenario involving the application of 3-D forces. Utilizing the three-tendon actuated robot detailed in Table I, we employ a device shown in Fig. 5 to apply various 3-D tip forces. The magnitude of the force is determined again using calibrated weights, while its direction is derived from the vector between the tip marker and another marker positioned at the upper part of the pulley, defining the force vector. We use in this case a weight of 65 g. We demonstrate in this section that with three actuators, we can estimate the three force components applied to the tip. Table III presents the results for different 3-D forces applied to the tip and Fig. 5 illustrates the shape of the manipulator. These results demonstrate an average force estimation accuracy of approximately 15.8% and an average RMSE of about 15 mm.

3) Estimation Distributed Force (Gravity): Finally, we tested our algorithm in order to estimate a distributed force along the soft robot for various configurations. It is important to note that accurately applying and measuring truly distributed loads for ground-truth purposes is challenging. Then, we assume that the magnitude of the gravity force is unknown and aims to estimate it. The objective is to simultaneously estimate the shape and the magnitude u_p of the gravity, assuming that $\boldsymbol{G} =$

TABLE II
EXPERIMENTAL RESULTS ESTIMATING 1-D EXTERNAL POINT FORCES

Planar deformation	$X_f = L/2$						$X_f = 3L/2$						$X_f = L$					
T (N)	1.90	3.45	4.78	0.54	4.47	5.85	2.0	3.28	4.54	2.56	4.44	6.9	1.36	1.70	1.95	2.97	3.11	3.42
y (mm)	-1.1	-11.0	-18.8	9.17	-9.2	-17.3	2.08	-5.65	-12.3	3.0	-4.56	13.8	5.0	4.92	4.92	-1.8	-1.5	-1.6
u_p^* (gF)	65	65	65	120	120	120	65	65	65	120	120	120	13	18	23	23	28	33
u_p (gF)	62.5	59.7	58.6	130.1	129.1	115.1	65.2	64.2	69.2	105.6	117.9	130.7	15.3	20.0	23.9	21.9	24.1	27.8
e_{u_p} (%)	3.9	9.7	9.8	8.5	7.6	4.1	0.3	1.3	6.4	11.9	1.8	8.9	17.6	11.3	4.0	5.0	13.9	15.9
RMSE (mm)	12.9	9.65	11.0	21.4	18.1	11.5	15.1	13.2	12.5	10.9	11.5	12.1	10.1	9.3	7.8	5.4	4.2	4.6
3-D deformation	$X_f = L/2$						$X_f = 3L/2$						$X_f = L$					
T (N)	1.38	2.72	4.18	2.48	4.15	7.61	1.3	2.8	4.8	1.9	3.4	5.1	4.86	5.1	5.2	1.2	1.4	0.9
y (mm)	-3.5	-11.9	-19.0	-7.5	-16.7	-29.9	-0.2	-9.0	-19.5	-1.3	-8.7	-16.9	-24.5	-24.5	-24.5	0.6	0.8	0.9
u_p^* (gF)	65	65	65	120	120	120	65	65	65	120	120	120	13	18	23	28	33	18
u_p (gF)	66.3	58.9	69.6	126.5	108.4	133.9	70.1	66.6	59.6	121.9	117.1	108.6	11.2	16.1	18.2	28.8	35.9	18.4
e_{u_p} (%)	2.0	9.4	7.1	5.5	9.7	11.6	7.9	2.5	8.4	1.6	2.4	9.5	13.9	10.6	21.1	2.8	9.0	2.2
RMSE (mm)	7.8	9.6	5.6	9.1	7.2	12.9	12.4	11.7	11.4	12.7	11.8	11.3	10.5	8.0	11.1	11.3	10.8	12.5

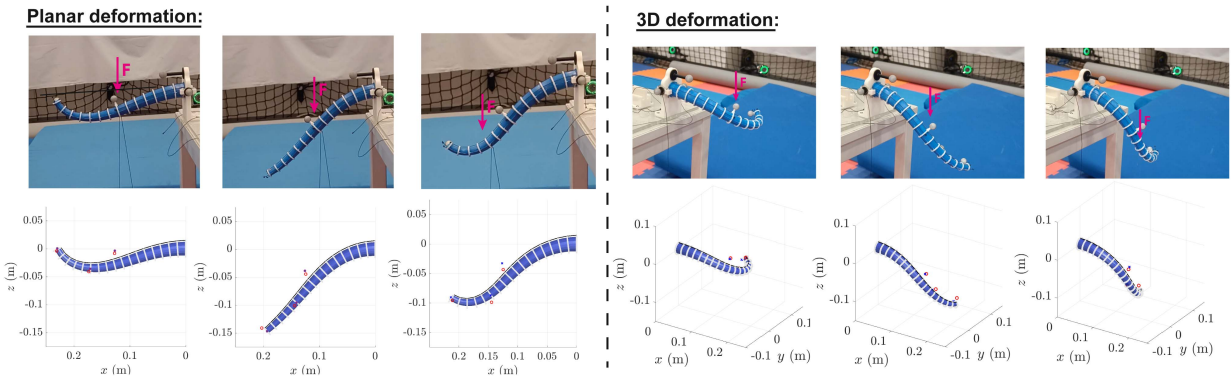

Fig. 4. Shape estimation for 1-D external point force under both planar and 3-D deformation.

TABLE III
EXPERIMENTAL RESULTS ESTIMATING 3-D EXTERNAL POINT FORCES

3-D tip force	1	2	3	4	5	6	7	8
$\boldsymbol{T}$ (N)	$[0,\ 2.50,\ 0]^T$	$[3.12,\ 4.87,\ 1.59]^T$	$[2.80,\ 7.30,\ 2.41]^T$	$[2.60,\ 0.86,\ 5.60]^T$	$[0.30,\ 2.79,\ 0.30]^T$	$[1.34,\ 5.72,\ 0.92]^T$	$[0.80,\ 0.6,\ 2.9]^T$	$[4.70,\ 1.60,\ 2.70]^T$
$\boldsymbol{y}$ (mm)	$[-2.6,\ 4.9,\ -6.6]^T$	$[2.2,\ -10.2,\ -16.4]^T$	$[4.8,\ -19.7,\ -15.9]^T$	$[-2.3,\ -18.9,\ -0.5]^T$	$[-1.3,\ 2.2,\ -9.4]^T$	$[-5.4,\ 6.5,\ -11.7]^T$	$[-0.5,\ -13.9,\ 7.7]^T$	$[-16.5,\ 5.8,\ -13.1]^T$
$\boldsymbol{u_p^*}$ (gF)	$[18.7,\ 52.7,\ 34.8]^T$	$[26.5,\ 53.0,\ -28.0]^T$	$[26.1,\ 56.2,\ -21.8]^T$	$[-19.7,\ -63.6,\ 17.1]^T$	$[19.6,\ 57.0,\ 25.6]^T$	$[14.7,\ 56.4,\ 31.8]^T$	$[-18.0,\ -64.0,\ 17.3]^T$	$[29.5,\ 50.5,\ 27.9]^T$
$\boldsymbol{u_p}$ (gF)	$[26.9,\ 58.4,\ 35.5]^T$	$[14.7,\ 52.2,\ -21.9]^T$	$[33.6,\ 51.4,\ -30.7]^T$	$[-14.2,\ -70.0,\ 15.6]^T$	$[22.7,\ 52.5,\ 23.9]^T$	$[4.8,\ 51.2,\ 31.5]^T$	$[-19.4,\ -55.7,\ 16.9]^T$	$[23.5,\ 40.2,\ 19.9]^T$
e_{u_p} (%)	15.0	20.0	19.2	13.6	8.7	16.9	12.1	22.1
RMSE (mm)	9.6	10.53	16.25	20.8	22.7	14.2	22.1	9.1

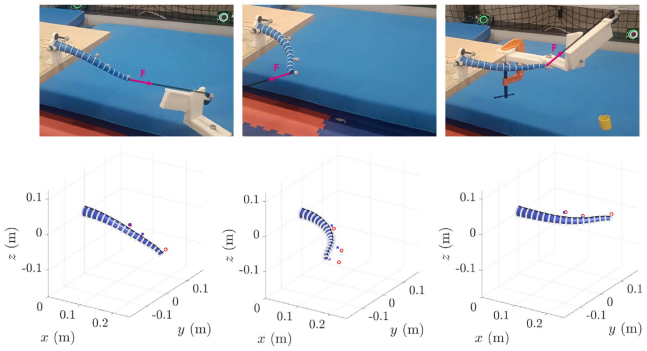

Fig. 5. Shape estimation for the case of 3-D external point forces.

TABLE IV
EXPERIMENTAL RESULTS ESTIMATING DISTRIBUTED FORCE (GRAVITY)

T (N)	0.88	1.50	2.01	2.64	3.34
y (mm)	0	-3.61	-6.57	-11.68	-16.2
u_p^* (KgF)	1	1	1	1	1
u_p (KgF)	0.92	1.04	1.1	1.01	0.97
e_{u_p} (%)	8.4	3.7	10.9	1.3	2.55
RMSE (mm)	6.42	2.15	3.14	5.97	9.28

$[0, 0, 0, 0, 0, -9.81]^T u_p$ of (8b). To achieve this, we conducted five experiments with different tendon actuation configurations (see Table IV). These results indicate a high accuracy in estimating the force and the shape of the manipulator, with an average force error of less than 5% and an RMSE of less than 10 mm.

4) Comparative Study of Model-Based Approaches for Soft Robot Estimation: The estimation-based methods in the literature enable robots to acquire sensing capabilities without increasing the structural complexity of continuum robots. Model-based methods require precise modeling of slender soft robots to accurately estimate their shape and external forces. Most existing model-based estimation approaches are simplified and based on constant curvature, piecewise constant curvature [42] assumptions, or on polynomial curvature [43]. However, very few have successfully accounted for all strain components simultaneously. To demonstrate the importance of using more complex models to precisely estimating external forces, we compare our method based in GVS, which considers bending, twisting, and elongation together, with a model that incorporates polynomial curvature in 3-D (3D-PC) and another that includes polynomial curvature in 3-D along with elongation (3D-PC+E). The experimental results, presented in Fig. 6, show

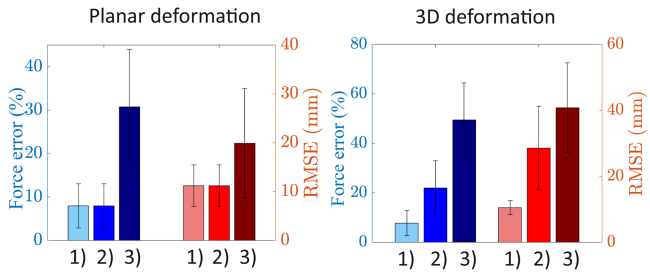

Fig. 6. Comparative results using different model-based approaches. (a) Our method based in GVS. (b) 3D-PC+E. (c) 3D-PC.

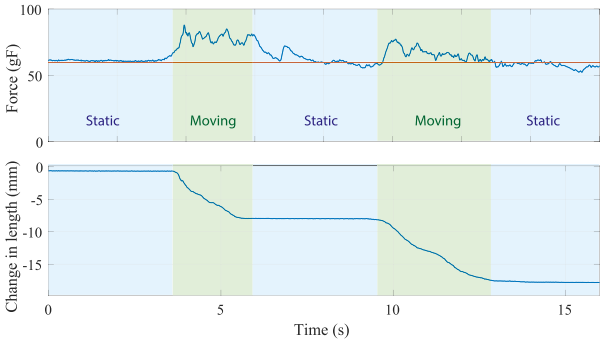

Fig. 7. Force estimation during dynamic tests.

the outcomes of the model-based approaches applied to the experiments of 1-D external point forces for both planar and out-of-plane deformations.

The results indicate that the proposed method achieves an average error of approximately 10% while the other methods exhibit errors of up to 30% in planar deformation and up to 50% in the 3-D case. In both cases, the findings highlight the importance of accounting not only for bending in 3-D but also for elongation to accurately estimate both the force and the shape. The 3-D deformation case further demonstrates that, in addition to elongation, incorporating twisting deformation is crucial for achieving high accuracy in the estimation.

C. Force Estimation During Dynamic Tests

In this section, we conducted an experiment in which the proposed approach was applied to estimate a 65 gF force applied at the middle of the soft robot while the system was in motion. In this experiment, the system is actuated using a single tendon-driven mechanism. We vary the actuator's length at different speed rates and also keep it static for certain periods. The results are shown in Fig. 7.

The average error during the static phase is 3%, while during the dynamic phase, the error increases to an average of 12% . In both cases, the method successfully estimates the force; however, its accuracy significantly decreases when the system is moving. In addition, in the first dynamic phase, the tendon is actuated with a reference speed of 3.5 mm/s, whereas in the second phase, it moves at 2.5 mm/s. As a result, the error in the second phase is lower despite the system being in motion. As expected, the estimation error increases as the dynamic effects

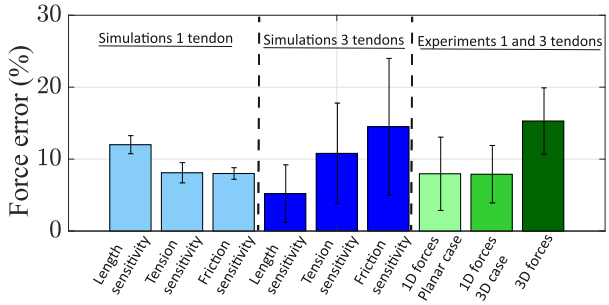

Fig. 8. Deviations errors obtained in the experimental and simulated data.

of the system become more significant. This is because our approach does not explicitly account for dynamic effects. In addition, we also validated the real-time capabilities of our shape estimation approach, achieving an average computation time of 0.167 ± 0.0463 s per sample. If faster performance is required for real implementations, then the method's speed could be improved by using the previous solution as the initial guess, adjusting the convergence tolerance, and optimizing the code for real-time calculation.

VI. Discussion and Conclusion

The aim of this study is to develop a novel method for estimating the forces and shape of slender soft robots. A key advantage of this method is its ability to utilize the tendons' length and tension directly for estimating both shape and external forces, eliminating the need for supplementary systems or bulky devices. Through multiple simulations, we illustrated the sensitivity of the proposed method to inaccuracies in length and tension measurements, as well as to inaccuracies in modeling friction in the tendons. Moreover, the method has been validated experimentally, demonstrating its effectiveness in estimating the force with an error of less than 10% for the 1-D case and around 15% for the 3-D case.

These values fall within the acceptable range in the soft robotics literature, particularly when using sensors embedded in the structure of the soft robot instead of a tracking position system. Specifically, if we compare our results with the only previous work that estimates force shape using only actuation measurements [35], we observe similar trend. This works report experiments for estimating 1-D external point forces for 98, 196, and 294 mN resulting in an average error of 6%. This error is within the range obtained in our study for 1-D external point forces (around 8%). For the case of 3-D external point forces, this is the first time such estimation has been reported in experiments using only actuation readings. While the error is slightly higher, it aligns with the sensitivity analysis conducted in Section IV. Fig. 8 presents both experimental and theoretical results on the same graph, showing the mean and standard deviations to clearly illustrate the errors and similarities between the experimental and simulated data.

For shape estimation, the error was less than 15 mm, which is 6% of the length of the prototype. The results also show that by increasing the number of tendons, more information can be

obtained, enabling the estimation of more complex forces. In addition, we did not observe higher tension introducing larger estimation errors. This is because the tendons operate within a range where they do not experience elongation. If the tendons were to elongate due to high tension values, this elongation would need to be included in the model, as it would affect the measured length within the robot and alter the friction direction, thereby introducing additional errors into the estimation algorithm. While the method has shown good accuracy and significant potential for applications requiring compact designs, it does have certain limitations that could be addressed in future research. The first limitation concerns the method's sensitivity to both the precision of sensor measurements. This suggests that improving the accuracy of the method would require to improve some parts of the prototype and use higher resolution measurements employing high-quality sensors that offer precise measurements with minimal noise and very high precision. Moreover, it would be beneficial to develop more accurate friction models.

The second limitation involves the assumption of knowing the force's position, which can restrict the method's applicability in certain scenarios. To address this, our future research will explore the integration of additional tendons to estimate more variables. Moreover, in future work, we plan to test this approach on more complex systems, such as chains of soft-rigid robots or soft robots that require modeling with multiple elements due to discontinuities in strain caused by discontinuous internal actuation or multiple point external forces.

APPENDIX
BASIC FORMULAE

Adjoint operator of $\mathfrak{se}(3)$

$$\mathrm{ad}_{\boldsymbol{\xi}(X)} = \begin{pmatrix} \widetilde{\mathbf{k}} & 0_{3\times3} \\ \widetilde{\mathbf{p}} & \widetilde{\mathbf{k}} \end{pmatrix}; \mathrm{ad}_{\boldsymbol{\eta}(\boldsymbol{X})} = \begin{pmatrix} \widetilde{\mathbf{w}} & 0_{3\times3} \\ \widetilde{\mathbf{v}} & \widetilde{\mathbf{w}} \end{pmatrix} \in \mathbb{R}^{6\times6}.$$

Adjoint map of $SE(3)$

$$\mathrm{Ad}_{\boldsymbol{g}(X)} = \begin{pmatrix} \boldsymbol{R} & 0_{3\times3} \\ \widetilde{\mathbf{r}}\boldsymbol{R} & \boldsymbol{R} \end{pmatrix} \in \mathbb{R}^{6\times6}.$$

Exponential map of $SE(3)$

$$\exp\left(\widehat{\boldsymbol{\Omega}}\right) = \boldsymbol{I}_4 + \widehat{\boldsymbol{\Omega}} + \frac{1}{\theta^2}\left(1-\cos\left(\theta\right)\right)\widehat{\boldsymbol{\Omega}}^2 + \frac{1}{\theta^3}\left(\theta-\sin\left(\theta\right)\right)\widehat{\boldsymbol{\Omega}}^3$$

where θ is $\|\mathbf{k}\|$. Moreover, fourth-order Zannah quadrature approximation of Magnus expansion

$$\boldsymbol{\Omega}_i(h) = \frac{h}{2}\left(\boldsymbol{\xi}_{iz1} + \boldsymbol{\xi}_{iz2}\right) + \frac{\sqrt{3}h^2}{12}\mathrm{ad}_{\boldsymbol{\xi}_{iz1}}\boldsymbol{\xi}_{iz2}$$

where subscripts "$z1$" and "$z2$" refer to quantities evaluated at the first and second collocation points: $X_i + (1/2 \mp \sqrt{3}/6)h$.

REFERENCES

[1] C. Laschi, B. Mazzolai, and M. Cianchetti, "Soft robotics: Technologies and systems pushing the boundaries of robot abilities," *Sci. Robot.*, vol. 3690, 2016, Art. no. eaah3690.

[2] D. Trivedi, A. Lotfi, and C. D. Rahn, "Geometrically exact models for soft robotic manipulators," *IEEE Trans. Robot.*, vol. 24, no. 4, pp. 773–780, Aug. 2008.

[3] C. Armanini, F. Boyer, A. T. Mathew, C. Duriez, and F. Renda, "Soft robots modeling: A structured overview," *IEEE Trans. Robot.*, vol. 39, no. 3, pp. 1728–1748, Jun. 2023.

[4] H. Abidi and M. Cianchetti, "On intrinsic safety of soft robots," *Front. Robot. AI*, vol. 4, 2017, pp. 1–6.

[5] D. Hu, F. Giorgio-Serchi, S. Zhang, and Y. Yang, "Stretchable e-skin and transformer enable high-resolution morphological reconstruction for soft robots," *Nature Mach. Intell.*, vol. 5, no. 3, pp. 261–272, 2023.

[6] D. Feliu-Talegon, Y. Abdullahi Adamu, A. T. Mathew, A. Y. Alkayas, and F. Renda, "Advancing soft robot proprioception through 6D strain sensors embedding," *Soft Robot.*, 2025, doi: 10.1089/soro.2024.0017.

[7] P. L. Anderson, A. W. Mahoney, and R. J. Webster, "Continuum reconfigurable parallel robots for surgery: Shape sensing and state estimation with uncertainty," *IEEE Robot. Automat. Lett.*, vol. 2, no. 3, pp. 1617–1624, Jul. 2017.

[8] S. Lilge, T. D. Barfoot, and J. Burgner-Kahrs, "Continuum robot state estimation using gaussian process regression on SE (3)," *Int. J. Robot. Res.*, vol. 41, no. 13-14, pp. 1099–1120, 2022.

[9] Y. Chitalia, N. J. Deaton, S. Jeong, N. Rahman, and J. P. Desai, "Towards FBG-based shape sensing for micro-scale and meso-scale continuum robots with large deflection," *IEEE Robot. Automat. Lett.*, vol. 5, no. 2, pp. 1712–1719, Apr. 2020.

[10] L. Xu, M. I. Miller, J. Ge, K. R. Nilsson, Z. T. H. Tse, and M. P. Fok, "Temperature-insensitive fiber-optic contact force sensor for steerable catheters," *IEEE Sensors J.*, vol. 16, no. 12, pp. 4771–4775, Jun. 2016.

[11] U. Seibold, B. Kubler, and G. Hirzinger, "Prototype of instrument for minimally invasive surgery with 6-axis force sensing capability," in *Proc. IEEE Int. Conf. Robot. Automat.*, 2005, pp. 496–501.

[12] S. H. Sadatiet al., "Stiffness imaging with a continuum appendage: Real-time shape and tip force estimation from base load readings," *IEEE Robot. Automat. Lett.*, vol. 5, no. 2, pp. 2824–2831, Apr. 2020.

[13] K. Xu and N. Simaan, "An investigation of the intrinsic force sensing capabilities of continuum robots," *IEEE Trans. Robot.*, vol. 24, no. 3, pp. 576–587, Jun. 2008.

[14] K. Xu and N. Simaan, "Intrinsic wrench estimation and its performance index for multisegment continuum robots," *IEEE Trans. Robot.*, vol. 26, no. 3, pp. 555–561, Jun. 2010.

[15] A. Y. Alkayas, D. Feliu-Talegon, A. T. Mathew, C. Rucker, and F. Renda, "Shape and tip force estimation of concentric tube robots based on actuation readings alone," in *Proc. 2023 IEEE Int. Conf. Soft Robot*, 2023, pp. 1–8.

[16] V. A. Aloi and D. C. Rucker, "Estimating loads along elastic rods," in *Proc. 2019 Int. Conf. Robot. Automat.*, 2019, pp. 2867–2873.

[17] M. A. Diezinger, B. Tamadazte, and G. J. Laurent, "3D curvature-based tip load estimation for continuum robots," *IEEE Robot. Automat. Lett.*, vol. 7, no. 4, pp. 10526–10533, Oct. 2022.

[18] S. Hasanzadeh and F. Janabi-Sharifi, "Model-based force estimation for intracardiac catheters," *IEEE/ASME Trans. Mechatron.*, vol. 21, no. 1, pp. 154–162, Feb. 2016.

[19] M. Khoshnam, A. C. Skanes, and R. V. Patel, "Modeling and estimation of tip contact force for steerable ablation catheters," *IEEE Trans. Biomed. Eng.*, vol. 62, no. 5, pp. 1404–1415, May 2015.

[20] J. Burgner-Kahrs, D. C. Rucker, and H. Choset, "Continuum robots for medical applications: A survey," *IEEE Trans. Robot.*, vol. 31, no. 6, pp. 1261–1280, Dec. 2015.

[21] R. Xu, A. Yurkewich, and R. V. Patel, "Curvature, torsion, and force sensing in continuum robots using helically wrapped FBG sensors," *IEEE Robot. Automat. Lett.*, vol. 1, no. 2, pp. 1052–1059, Jul. 2016.

[22] F. Khan, R. J. Roesthuis, and S. Misra, "Force sensing in continuum manipulators using fiber Bragg grating sensors," in *Proc. 2017 IEEE/RSJ Int. Conf. Intell. Robots Syst.*, 2017, pp. 2531–2536.

[23] D. C. Rucker and R. J. Webster, "Deflection-based force sensing for continuum robots: A probabilistic approach," in *Proc. 2011 IEEE/RSJ Int. Conf. Intell. Robots Syst.*, 2011, pp. 3764–3769.

[24] A. Bajo and N. Simaan, "Kinematics-based detection and localization of contacts along multisegment continuum robots," *IEEE Trans. Robot.*, vol. 28, no. 2, pp. 291–302, Apr. 2012.

[25] Q. Qiao, G. Borghesan, J. De Schutter, and E. V. Poorten, "Force from shape—estimating the location and magnitude of the external force on flexible instruments," *IEEE Trans. Robot.*, vol. 37, no. 5, pp. 1826–1833, Oct. 2021.

[26] V. Aloi, K. T. Dang, E. J. Barth, and C. Rucker, "Estimating forces along continuum robots," *IEEE Robot. Automat. Lett.*, vol. 7, no. 4, pp. 8877–8884, Oct. 2022.
[27] J. M. Ferguson, D. C. Rucker, and R. J. Webster, "Unified shape and external load state estimation for continuum robots," *IEEE Trans. Robot.*, vol. 40, pp. 1813–1827, Feb. 2024.
[28] S. Zaidi, M. Maselli, C. Laschi, and M. Cianchetti, "Actuation technologies for soft robot grippers and manipulators: A review," *Curr. Robot. Rep.*, vol. 2, no. 3, pp. 355–369, 2021.
[29] A. L. Orekhov, E. Z. Ahronovich, and N. Simaan, "Lie group formulation and sensitivity analysis for shape sensing of variable curvature continuum robots with general string encoder routing," *IEEE Trans. Robot.*, vol. 39, no. 3, pp. 2308–2324, Jun. 2023.
[30] J. Li, F. Zhang, Z. Yang, Z. Jiang, Z. Wang, and H. Liu, "Shape sensing for continuum robots by capturing passive tendon displacements with image sensors," *IEEE Robot. Automat. Lett.*, vol. 7, no. 2, pp. 3130–3137, Apr. 2022.
[31] Z. Liu, Z. Cai, H. Peng, X. Zhang, and Z. Wu, "Morphology and tension perception of cable-driven continuum robots," *IEEE/ASME Trans. Mechatron.*, vol. 28, no. 1, pp. 314–325, Feb. 2023.
[32] D. Feliu-Talegon, A. T. Mathew, A. Y. Alkayas, Y. A. Adamu, and F. Renda, "Dynamic shape estimation of tendon-driven soft manipulators via actuation readings," *IEEE Robot. Automat. Lett.*, vol. 10, no. 1, pp. 780–787, Jan. 2025.
[33] Z. Wang, X. Wei, X. Yu, Z. Jia, S. Qian, and D. Wang, "Data-based shape self-sensing of a cable-driven notched continuum mechanism using multi-dimensional intrinsic force information for surgical robot," *J. Mechanisms Robot.*, vol. 16, no. 7, 2024, Art. no. 071002.
[34] F. Feng, W. Hong, and L. Xie, "A learning-based tip contact force estimation method for tendon-driven continuum manipulator," *Sci. Rep.*, vol. 11, no. 1, 2021, Art. no. 17482.
[35] F. Duet al., "A sensor-free force estimation method for notched continuum surgical robot," *IEEE/ASME Trans. Mechatron.*, vol. 30, no. 2, pp. 1424–1434, Apr. 2025.
[36] A. T. Mathew, I. B. Hmida, C. Armanini, F. Boyer, and F. Renda, "Sorosim: A MATLAB toolbox for hybrid rigid–soft robots based on the geometric variable-strain approach," *IEEE Robot. Automat. Mag.*, vol. 30, no. 3, pp. 106–122, Sep. 2023.
[37] F. Renda, C. Armanini, A. Mathew, and F. Boyer, "Geometrically-exact inverse kinematic control of soft manipulators with general threadlike actuators' routing," *IEEE Robot. Automat. Lett.*, vol. 7, no. 3, pp. 7311–7318, Jul. 2022.
[38] F. Boyer and F. Renda, "Poincare's equations for cosserat media: Application to shells," *J. Nonlinear Sci.*, vol. 27, no. 1, pp. 1–44, 2017.
[39] A. T. Mathew, D. Feliu-Talegon, A. Y. Alkayas, F. Boyer, and F. Renda, "Reduced order modeling of hybrid soft-rigid robots using global, local, and state-dependent strain parameterization," *Int. J. Robot. Res.*, vol. 44, no. 1, pp. 129–154, 2025.
[40] W. S. Rone and P. Ben-Tzvi, "Continuum robot dynamics utilizing the principle of virtual power," *IEEE Trans. Robot.*, vol. 30, pp. 275–287, Feb. 2014.
[41] H. Li, L. Xun, and G. Zheng, "Piecewise linear strain cosserat model for soft slender manipulator," *IEEE Trans. Robot.*, vol. 39, no. 3, pp. 2342–2359, Jun. 2023.
[42] R. J. Webster and B. A. Jones, "Design and kinematic modeling of constant curvature continuum robots: A review," *Int. J. Robot. Res.*, vol. 29, no. 13, pp. 1661–1683, 2010.
[43] C. D. Santina and D. Rus, "Control oriented modeling of soft robots: The polynomial curvature case," *IEEE Robot. Automat. Lett.*, vol. 5, no. 2, pp. 290–298, Apr. 2020.

Daniel Feliu-Talegon received the M.Sc. and Ph.D. degrees in control engineering from the University of Castilla La Mancha, Spain, in 2014 and 2019, respectively.

He is currently a Postdoctoral Fellow with the Cognitive Robotics department, Delft University of Technology, Delft, The Netherlands. His research interests include the fractional dynamics and control systems, dynamic control of flexible robots, control of lightweight manipulators in aerial robotics, and sensorization, control, and modeling of soft robot manipulators and deformable objects.

Abdulaziz Y. Alkayas received the B.Sc. degree in electromechanical engineering from Alexandria University, Alexandria, Egypt, in 2019, and the M.Sc. degree in mechanical engineering in 2021 from Khalifa University, Abu Dhabi, UAE, where he is currently working toward the Ph.D. degree in mechanical engineering.

His research interests include modeling and control of dynamical systems, soft robotics, and the application of machine learning techniques.

Yusuf Abdullahi Adamu received the B.Eng. degree in mechanical engineering from Bayero University Kano, Kano, Nigeria, in 2013, and the M.Eng. degree in mechatronics engineering from the University of Malaya, Kuala Lumpur, Malaysia, in 2019. He is currently working toward the Ph.D. degree in engineering with a concentration in robotics with Khalifa University, Abu Dhabi, United Arab Emirates.

His research interests include prototyping, sensorization, and modeling of soft robot manipulators

Anup Teejo Mathew received the Ph.D. degree in mechanical engineering from the National University of Singapore, Singapore, in 2019.

He is currently a Postdoctoral Fellow with Khalifa University, Abu Dhabi, United Arab Emirates. He has authored or coauthored several papers on topics ranging, such as soft robotics modeling, electroactive polymers, and energy harvesting. His current research interests include theoretical modeling of soft robotics and design and development of underwater soft robotics.

Federico Renda received the B.Sc. and M.Sc. degrees in biomedical engineering from the University of Pisa, Pisa, Italy, in 2007 and 2009, respectively, and the Ph.D. degree from the BioRobotics Institute of Scuola Superiore Sant'Anna, Pisa, in 2014.

He is currently an Associate Professor with the Department of Mechanical and Nuclear Engineering, Khalifa University, Abu Dhabi, United Arab Emirates. Before joining Khalifa University, he was a Postdoctoral Fellow with the BioRobotics Institute of Scuola Superiore Sant'Anna. His research focuses on the study of multibody dynamical systems, including modeling and control of complex soft and underwater robots.

Dr. Renda has been appointed as an Associate Editor and Program Committee Member of important robotics journals and conferences, such as the *International Journal of Robotics Research* and the International Conference on Robotics and Automation.